

Investigations on the role of Ni-catalyst for the VLS growth of quasi-aligned GaN nanowires by chemical vapor deposition

V. Purushothaman · K. Jeganathan

Received: 3 April 2013 / Accepted: 10 June 2013 / Published online: 22 June 2013
© Springer Science+Business Media Dordrecht 2013

Abstract We report the fabrication of quasi-aligned GaN nanowires (NWs) on Si(111) substrate by chemical vapor deposition using Ni as a catalyst. The structural and composition analysis of Ni-catalyst on the apex of the GaN NWs were investigated using high-resolution transmission electron microscopy and energy dispersive X-ray spectroscopy. The catalyst contains only Ni–Ga alloy with the composition of ~66:33 having Ni₃Ga phase. GaN NWs exhibit wurtzite structure without any amorphous sheath layer or cubic inclusions, where the catalyst contains the mixture of both the crystalline and amorphous phases. During growth, the nitrogen radicals are expected to migrate on the surface of the catalytic droplet to incorporate into the growing lattice via the solid–liquid interface due to poor solubility of N in Ni, which forbids the alloying of nitrogen with Ni. Temperature-dependent photoluminescence reveals that the intensity of donor-bound exciton (D⁰X) peak consistently increases with a blue shift as the temperature decreases. The D⁰X peak is centered at 3.467 eV for 10 K. Interestingly, yellow band, the characteristic nature of defects-induced luminescence, is absent in Ni-catalytic-assisted growth of GaN NWs.

Keywords Gallium nitride · Nanowires · Chemical vapor deposition · Vapor–liquid–solid mechanism · Photoluminescence

Introduction

Nanostructured materials have attracted extensive interest over the past decade due to the importance in both fundamental research and the development of new generation nanodevices (Yan et al. 2009; Duan et al. 2003; Byeun et al. 2006). Nanowires (NWs) explore a novel way to fabricate devices with a bottom-up approach instead of conventional top–down methods (Cui et al. 2003). The fabrication of self-assembled NWs is of great interest for the continued miniaturization of electronics (Duan et al. 2001). Further, the integration of III–V NWs and silicon (Si) holds a significant promise for novel nanoscale electronic, photonic, or optoelectronic devices. Such hybrid nanostructures would bridge the gap between high-performance direct band gap compound semiconductors with well-matured and inexpensive Si technology (Ra et al. 2013). Gallium nitride (GaN) with a direct and wide band gap of 3.4 eV at room temperature has been considered as an ideal material for the fabrication of high-brightness visible light-emitting diodes (Kuykendall et al. 2003), laser diodes (Gradecak et al. 2005), and high-power integrated circuits (Huang et al. 2002). Different techniques, such as hydride vapor phase epitaxy (Lekhal et al. 2012), MBE (Debnath et al.

V. Purushothaman · K. Jeganathan (✉)
Centre for Nanoscience and Nanotechnology,
School of Physics, Bharathidasan University,
Tiruchirappalli 620 024, India
e-mail: kjeganathan@yahoo.com

2007), and CVD (Kuykendall et al. 2003), have been widely employed to fabricate GaN NWs with extremely high-crystalline quality. For instance, GaN NWs grown by MBE were shown to have high-optical quality with strong luminescence efficiency (Robins et al. 2007). However, the MBE system has some limitations with the large-scale production, slow growth rate, and very expensive, further it requires ultra-high vacuum. CVD, a principal technique for growing III-nitrides, offers several advantages such as low cost, large-scale production, and reproducibility. For future commercial device applications, fabrication of aligned nanostructures with high density is very important because they can be effectually incorporated into the building blocks of the nanodevices. A variety of semiconductor NWs have been synthesized by the vapor–liquid–solid (VLS) mechanism (Wagner and Ellis 1964), which makes use of a foreign catalyst elements (metals such as Au, Ni, Pt, etc.) for the nucleation and growth of NWs. VLS offers a low-cost method and size controllable growth of a semiconductor NWs. The anisotropic growth rate of NWs is enhanced by the presence of catalyst on the apex of the wire, which is considered as the characteristics of VLS approach. The role of catalyst for the fabrication of NWs under VLS approach is very significant as it holds the key for the control of diameter and distribution of NWs besides good optical and crystalline quality of NWs. Nickel catalyst has been widely employed for the fabrication of GaN NWs (Chèze et al. 2010a, b, c; Lari et al. 2008; Weng et al. 2009; Geelhaar et al. 2007; Lekhal et al. 2012; Zhou et al. 2012). Despite the advantage of Ni catalyst, there are some important issues yet to be addressed, for example, chemical and crystalline nature of the catalyst droplet and basic growth mechanism whether VLS or VSS or mixture of both are not clearly available in the literature. (Diaz et al. 2012) have argued that the growth of GaN NWs grown by chemical vapor deposition was governed by the VLS mechanism. On the other hand, (Weng et al. 2009), have demonstrated that GaN NW growth by MOVPE at 900 °C was driven by VSS mechanism. In literature, MBE growth of Ni-catalyst-assisted GaN NWs have demonstrated that the growth proceeds through the VSS mechanism (Chèze et al. 2010a, b, c). However, these results could not be compared with the CVD grown NWs as the MBE growth was carried at a low temperature of ~ 750 °C. In addition, the importance of III/V ratio for the growth of GaN NWs is rarely

explored in thermal chemical vapor deposition (Cai et al. 2006). Investigations on the role of catalyst for the formation of NWs will be very essential to understand the growth kinetics, doping effects, and formation of abrupt interfaces (Wen et al. 2009) for the advances in the anisotropic fabrication of one-dimensional NWs under VLS approach. Hence, we report the fabrication of Ni-catalyst-assisted, quasi-aligned GaN NWs on Si(111) substrate by chemical vapor deposition. The structure and chemistry of the Ni-catalyst particles that terminate GaN NWs were investigated using a combination of electron diffraction, high-resolution transmission electron microscopy, and X-ray energy dispersive spectrometry.

Experimental

GaN NWs were grown on Ni-coated Si(111) substrates using a metal Ga (ALFA AESAR make-99.999 %) as source material and NH_3 as reactant gas in a two zone tubular furnace at atmospheric pressure by chemical vapor deposition technique. Nitrogen (500 Cubic centimeter per minute (SCCM)) is used as the carrier gas to transport the metal Ga to the substrate. Both the source and the substrate temperatures were kept at 900 °C, and the growth duration is fixed for 30 min. In all the experiments, the source to the substrate distance was maintained at 10 mm. Prior to loading, the Si substrates were cleaned by standard RCA cleaning procedure and pre-coated with 5-nm thick Ni-film by e-beam evaporation technique. Then, the substrates were annealed at 900 °C under vacuum (1×10^{-3} mbar) for 15 min to form Ni droplets. In order to investigate the impact of III/V ratio on the morphological change in NWs, ammonia flow rate has been varied between 200 and 100 SCCM.

The morphology and compositional analyses of GaN NWs were studied using a field emission scanning electron microscopy (FESEM) (Carl Zeiss-Sigma) equipped with energy dispersive X-ray analysis (EDX) (Oxford instruments). EDX has been recorded using the point and identification tool with an accelerating voltage of 10 keV and achieved the point resolution of ~ 2 nm. High-resolution transmission electron microscope (HRTEM) (JEOL-2010—200 kV—equipped with LaB6 Gun—Point to point resolution of 0.19 nm) was carried out to examine the crystallinity of a single GaN NW. TEM samples were

prepared by scratching GaN NWs from the substrate, dispersing them in ethanol, and casting a drop of the suspension on a Cu-grid coated with porous carbon thin film. Optical characteristics of the ensemble of NWs were recorded using temperature-dependent photoluminescence. PL spectra for NWs were collected using a monochromator (Horiba Jobin–Yvon—0.55 M), with 325 nm He–Cd laser focused through an objective lens, and the resulting laser spot incident on the sample had a diameter of $\sim 10 \mu\text{m}$. Luminescence signal from the sample is collected through a charge-coupled device (CCD). The sample is placed in a closed cycle He cryostat with the temperature variable between 10 and 300 K.

Results and discussion

Figure 1a shows the schematic representation of CVD reactor in which the substrate is placed downstream to the Ga source and the bottom part of the image represents the temperature profile for the CVD reactor. The CVD reactor is home-built and customized to achieve the flat central zone for 15–20 cm. Figure 2 shows the XRD pattern recorded for the GaN NWs grown for 30 min at 900 °C under the NH_3 flow rate of 200 SCCM. All the peaks can be indexed to the wurtzite GaN (JCPDS Card No: 898624) with the dominant diffraction peaks located at $2\theta = 32.14^\circ$, 34.21° , and 36.47° corresponding to (100), (002), and (101) planes, respectively, which indicates that the NWs are quasi-aligned and free of any cubic inclusions. Further, the peak position substantiates the strain-free nature of the NWs besides good crystalline quality. In addition to wurtzite GaN peaks, SiN and SiO_2 peaks were also found from the XRD results. Here, the peak corresponds to SiN has been attributed to the nitridation of Si at higher temperature (Stoica et al. 2008). Despite RCA cleaning of Si substrate, the sample transfer through atmosphere prior to Ni and GaN deposition results in oxidation, and the peak at 26.06° is assigned to the native oxide (SiO_2) of Si.

Figure 3a, b shows the FESEM images of Ni-catalyst droplet on the Si(111) substrate after annealing at 900 °C for 15 min under vacuum (1×10^{-3} mbar). The self-assembly of Ni nanodroplets after annealing is appeared to be irregular in shape and size. Inset of Fig. 3a shows the histogram of size distributions of Ni nanoparticles. The average diameter of the droplet is

~ 50 nm. The size and the shape of Ni droplets on silicon substrate is strongly influenced by a contact angle, and balance of the forces of surface tension and interfacial energies of liquid–solid (Roper et al. 2010). Figure 3c, d shows the tilt-view FESEM images of early stage of nucleation formed during the exposure of Ga metal flux at 900 °C with NH_3 flow rate of 200 SCCM for 5 min. After the exposure of metal Ga and reactive NH_3 , the average size of the droplet is found to be increased to 90 nm (inset of the Fig. 3c shows the histogram for the size distribution), and the droplets tend to become regular in shape irrespective of size. As a nucleation begins to form, its size augments to 90 nm besides enhancement of height. As the Ga and NH_3 supply continues, the supersaturation at the liquid–solid interface leads to the axial growth of NWs. Figure 3e, f shows the tilt-view FESEM images of the high-yield straight and quasi-aligned GaN NWs grown on Si(111) substrates. The average diameter and length of the NWs were ~ 120 nm and 5 μm , respectively, for the NWs grown with the 200 SCCM of NH_3 . The calculated average axial growth rate is 165 nm/sec. The inset of Fig. 3f shows the plot for diameter versus length of GaN NWs. The diameter of the NWs does not show any visible change from top to bottom or in other words the NWs are free from tapering effect. Figure 3g, h shows the Ni–Ga droplet on top of the NW which is the characteristic of catalytic-assisted VLS growth mechanism.

Inset of 3f shows the plot for diameter versus length for NWs grown for the duration of 30 min (totally 200 NWs were considered). The length and diameter does not have a considerable relationship for the given growth conditions, from which we can conclude that the NWs growth rate is independent of the diameter. In general, VLS growth is driven by the two important pathways of adatoms through, (i) direct impingement and (ii) the surface diffusion (Harm et al. 2007; Dubrovskii et al. 2009). For the diffusion-induced growth modes, NWs exhibit tapering effect due to lateral overgrowth, as the NW length is higher than the adatom diffusion length, and hence, the growth rate would become dependent on the diameter of the wire (Dubrovskii et al. 2009). Under this circumstance, the NW growth rate is a function of diameter governed by Gibbs–Thomson effect (Seifert et al. 2004). However, for the NWs growth with larger catalytic particles under high supersaturation, the Gibbs–Thomson effect can be neglected, which is responsible for this peculiar

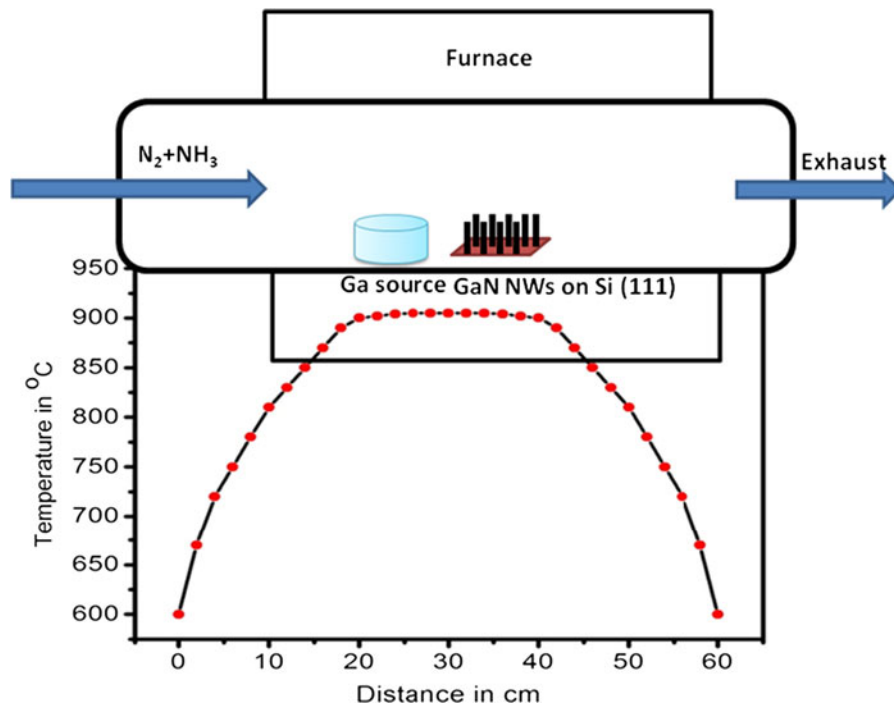


Fig. 1 The schematic representation of two zone chemical vapor deposition (CVD) reactor. The *bottom* part shows the temperature profile of the reactor

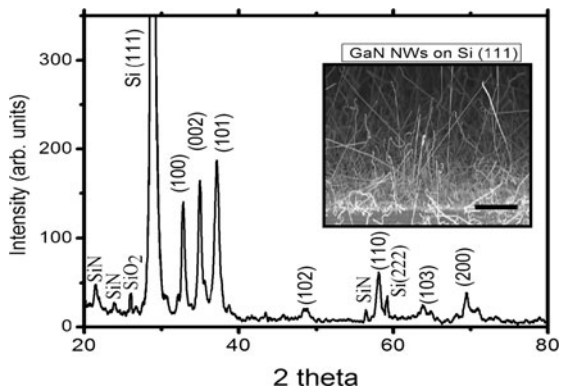


Fig. 2 X-ray diffraction pattern recorded on the ensemble of GaN NWs. The *inset* shows the FESEM image of GaN NWs (Scale=5 μm)

phenomenon of diameter independent growth rate (Kodambaka et al. 2006).

In a typical thermal CVD reactor, certain parameters are very imminent for the growth of GaN NWs. As the distance between the source (metal Ga) and the substrate is kept at 10 mm, the Ga vapor pressure constantly changes with time that leads to the variation

of III/V ratio in local growth regime. The high-vapor pressure of Ga at the initial stage of the growth is expected to promote Ga-rich conditions. However, the growth regime may change from Ga-rich to N-rich conditions after a certain period of NH_3 exposure as the Ga stabilizes. In addition to the variation of vapor pressure with time, the top layer of source metal Ga reacts with the N-radicals to form a thin layer of GaN on the source, which further reduces the Ga evaporation. Hence, the N-rich growth regime is expected in the consecutive growth of NWs. After the prolonged growth duration, the evaporation of Ga almost stops at which the NW growth may be ceased. This clearly demonstrates that in a typical CVD reactor with metal Ga and NH_3 as the precursors, the growth starts with Ga-rich condition, proceeds under the N-rich and ends with Ga nil condition (no further growth is possible for the extended time of growth).

The NWs growth occurs at different rates as the III/N ratio continuously change with time in growth front. First, we analyze the initial growth condition that proceeds under Ga-rich conditions. The average diameter of the as annealed Ni-nanoparticles on

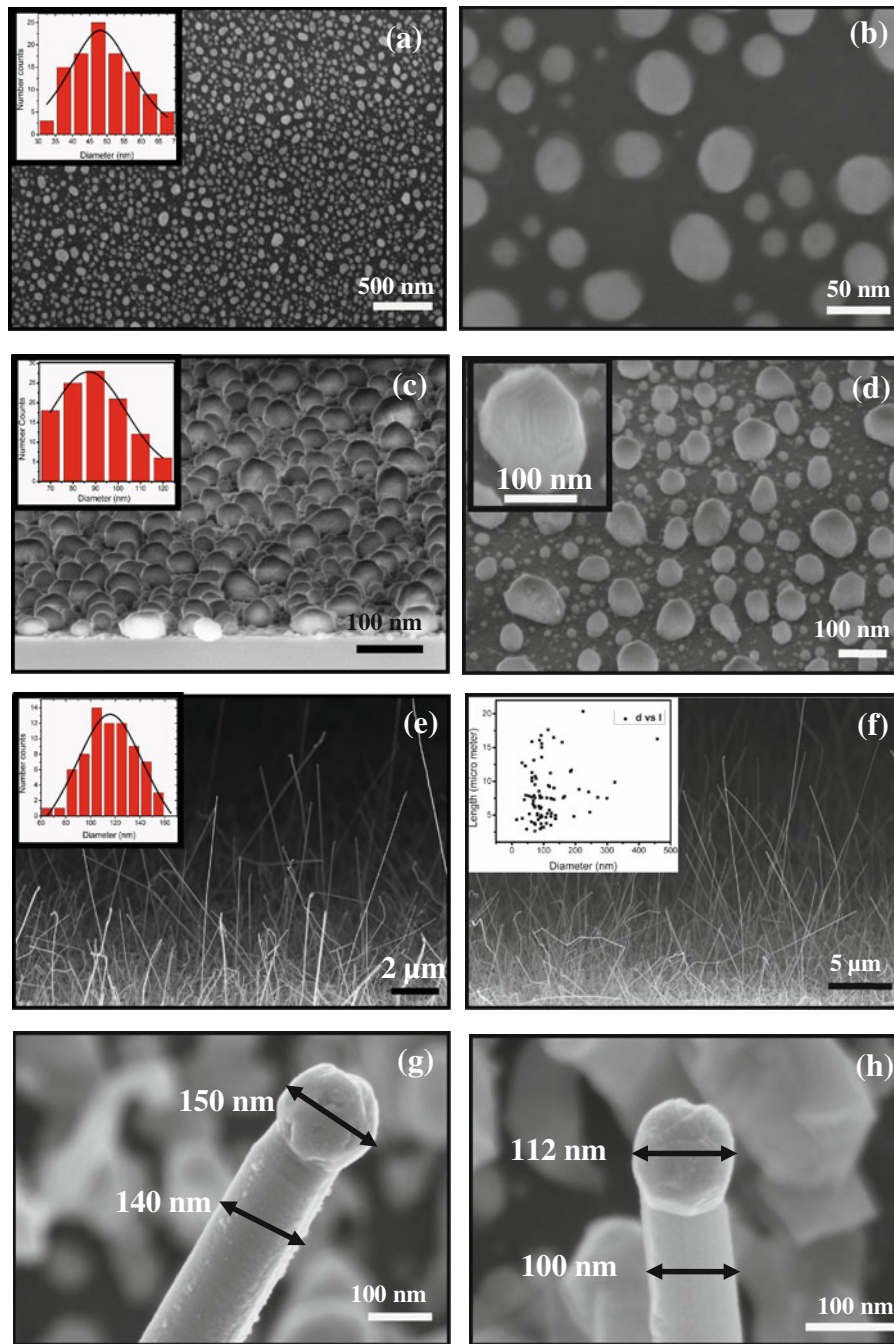


Fig. 3 **a, b** The Ni nanodroplets on Si(111) with different magnification and the *inset* shows the size distribution of Ni nanodroplets; **c** shows the Ni+ GaN nucleation after the reaction of Ga and NH₃ for 5 min, and the *inset* shows the size distribution of the droplets; **d** shows the magnified view of the droplet and the droplet reveals the hexagonal pattern; **e, f** shows

the quasi-aligned GaN NWs grown with 200 SCCM of NH₃ having the average diameter and length is ~ 120 nm and 5 μm, respectively, and the *inset* shows the size distribution the GaN NWs; **g, h** shows a clear Ni-catalyst droplet on the apex of the NW

Si(111) substrate before loading into the CVD chamber is ~ 50 nm (Inset of Fig. 3a). The supply of Ga and NH_3 for 5 min, the GaN nucleation is formed having an average diameter of ~ 90 nm, which is twice the diameter of the catalyst particle. It is obvious that the Ga reacts with Ni to form Ni–Ga alloy, which increases the diameter of the alloy droplets. Inset of the Fig. 3d shows the focused view of GaN nucleation, in which the hexagonal pattern on the surface of the droplet is clearly visible. During the early stage of the growth under Ga-rich conditions, the growth results in negligible increment on the axial direction, but greatly increases the radial growth (Geelhaar et al. 2007). However, the average diameter of the GaN NWs was 120 nm for the growth duration of 30 min (Inset of Fig. 3e shows the histogram for the diameter distribution of GaN NWs). The increase of NWs diameter as compared to the Ni droplet and nuclei can intimately be related to the initial nucleation conditions, such as reactor pressure and incorporation rate of radicals. It is worth noting that the incorporation rate of Ga and N radicals into growing lattice through Ni-droplet depends on the Ni–Ga binary phase diagram. However, the solubility of nitrogen in Ni is negligible, and hence, Ga expected to dissolve to form

a stable phase of Ni_3Ga (Gröbner et al. 1999). Hence, the Ga-rich growth regime is maintained at the solid–liquid interface, and the similar situation is expected to be retained, even as the growth regime transforms to N-rich conditions. Despite the Ga-rich at the growth interface, the crystallization strongly depends on the availability of nitrogen radicals. As nitrogen has poor solubility in Ni–Ga alloy, nitrogen radicals may incorporate into the growing GaN lattice at the solid–liquid interface, which is primarily responsible for the axial growth of NWs. Thus, the NW formation is governed by the diffusion of Ga radicals through Ni–Ga alloy droplet, and the incorporation of N-radicals at the solid–liquid interface for the given domain of the growth parameters.

Further, in order to understand the importance of NH_3 flow rate, in turn varies III/V ratio in the growth of NWs, we have grown GaN NWs with reduced NH_3 supply of 100 SCCM. Figure 4a–d shows the corresponding FESEM images of GaN NWs grown at 100 SCCM of NH_3 with the identical parameters of Fig. 3e. The average diameter and length of the NWs are 160 nm and 4 μm , respectively. The average growth rate of the NWs is 130 nm/min. Here, the reason for increase of diameter can be understood that

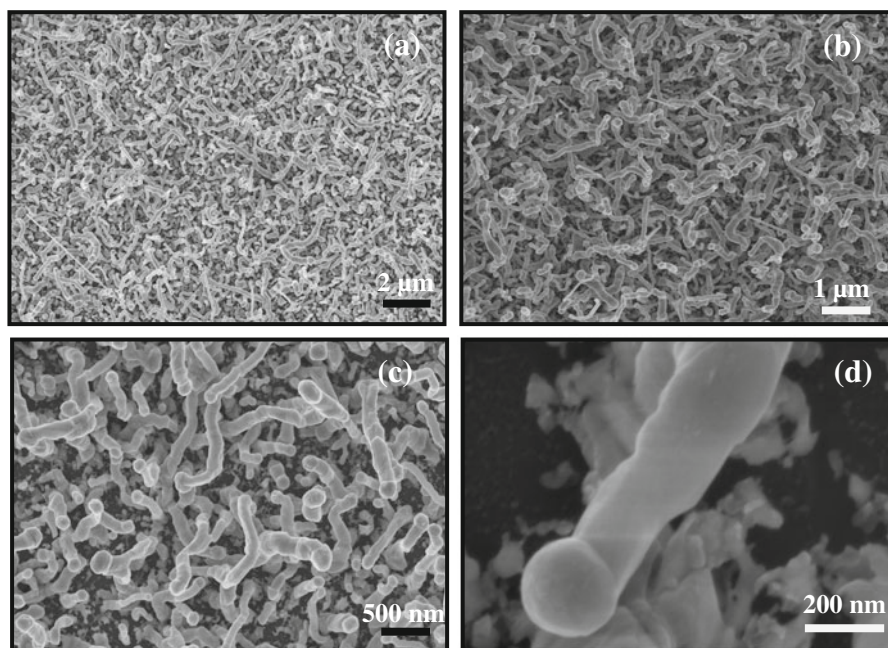


Fig. 4 a–d FESEM images of GaN NWs grown under the NH_3 flow rate of 100 SCCM. It is worth to note that the NWs grown with reduced NH_3 (100 SCCM) have higher diameter and lower growth rate as compared with the NWs grown with 200 SCCM of NH_3

the growth of GaN takes place under Ga-rich conditions, as the NH_3 supply decreases which increases the radial growth as compared to the NWs grown with 200 SCCM of NH_3 . Similar, the average length of the NWs is smaller than that of N-rich grown NWs, which suggests that N-radicals has a major contribution for the growth rate. In addition, the NWs are entangled and tapered, as compared to Fig. 3e, as the migration length of N-radicals is considerably reduced under Ga-rich conditions.

In order to probe the chemical composition of the NW EDX in combination with high-resolution FESEM have been recorded on different places including catalytic droplet, interface between the wire and droplet, and the body of the NW. A point and identification tool is employed to achieve a 2-nm resolution for composition analysis along the axial direction of NW. Figure 5a–c shows the high-resolution FESEM in combination with EDX spectra recorded on the various parts of GaN NW and catalytic droplet. In the FESEM image, the points (spectrum 1, 2, 3) denote the place where the EDX has been recorded. The brighter contrast of the catalyst particle than that of the NW indicates that the particle has a higher average atomic number, or the particle is thicker than the NW in the viewing direction. In central region of droplet, the point scan indicates the presence of both Ga and Ni with an average of 27 ± 3 and 73 ± 3 at.%, respectively. This value is consistent with the equilibrium phase of α' - Ni_3Ga or Ni–Ga solid solution (Venugopalan et al. 1997). Nitrogen is not observed in the droplet within the detection limit of EDX. This observation reflects the relatively poor solubility of N in Ni, and corroborates that Ni_3N is not a stable phase and decomposes into Ni and N_2 at above 600 °C (Wriedt 1991). In addition to Ni_3Ga phase, there are possibilities for the formation of other meta stable phases, such as Ga_3Ni_2 , which depend on the Ga vapor pressure. As we have already noticed, the initial growth contains Ga-rich condition, the possibility for other phases could not be ruled out. The Ga_3Ni_2 phase could enable an invariant equilibrium with Ni–Ga and exhibit liquid phase during growth, as indicated in the Ni–Ga phase diagram at 895 °C, which facilitate the growth under VLS approach (Chèze et al. 2010a, b, c). It is speculated that the catalytically active meta stable Ga_3Ni_2 phase could attain the thermo dynamical equilibrium phase of Ni_3Ga during cooling process due to the absence of Ga radials for the diffusion into

the catalyst, as supported by the post growth analysis. Further, the distribution of oxygen indicates the presence of oxide shell like around the seed which contains both Ga and Ni. The oxide shell is most likely formed due to the post growth exposure of GaN NWs to the ambient atmosphere. EDX recorded at the interface of the droplet shows Ni, Ga, and N with the ratio of Ni:Ga:N—60:25:15 at.%, which clearly demonstrates that the interface consists of both GaN and Ni–Ga solid solution, in which Ni is dominant. As the point and ID is slightly moved toward the body of the NW (with 5 nm), the Ni concentration is almost vanished and the Ga and N are present dominantly with the ratio of Ga:N 48:52 at.%. Figure 5d shows the plot for the atomic percentage versus distance (nm) from the top of the catalyst droplet toward the body of the NW. From the plot, it is clear that the atomic percentage of Ni suddenly reduces at the catalyst–NWs interface and almost vanished in the body of the GaN NW. Despite the favorable solid-solution of Ni–Ga at the interface, Ni catalyst does not migrate into the crystal lattice of GaN at least with the detection limit. This data contradicts to the earlier report (Venugopalan et al. 1997) of GaN NWs grown by MBE using Ni catalyst at low temperature (730 °C), in which the formation of extended defects is ascribed to the possible incorporation of Ni impurities into the crystal lattice due to immiscible Ni–Ga binary phase at 730 °C. However, our results demonstrate that the stacking faults can be suppressed for the GaN NWs grown at relatively high temperature using Ni catalyst, as substantiated by HRTEM and EDX measurements on single GaN NW. We have performed numerous experiments and the results of all the samples, including the morphology and its characteristics show very similar results with high reproducibility for the given experimental conditions.

In order to establish the growth mechanism, in situ and ex situ analyses are very important. Accurate droplet analysis by in situ measurement is impossible in thermal CVD reactor because of the hot walls required for the stabilization of gaseous species. When the Ni–Ga droplet is Ga rich (>60 %), the alloy composition is expected to be the mixture of solid and liquid phases (Ducher et al. 2007). HRSEM–EDX measurements show that the post growth catalyst particle contains ~ 70 % of Ga and 30 % Ni. Although, the ex situ EDX results do not reflect the actual composition of the catalyst particle during the

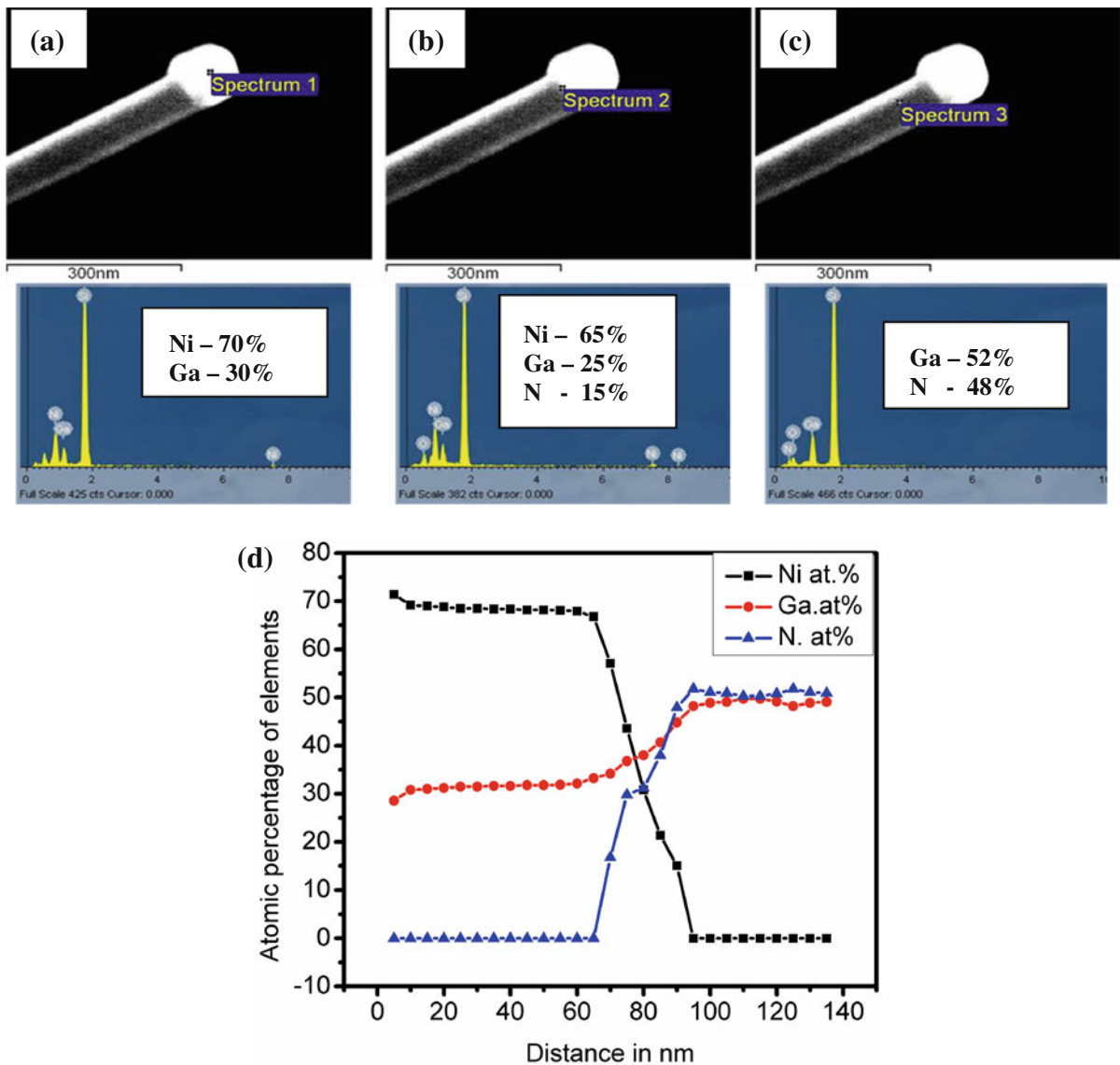


Fig. 5 High-resolution FESEM image shows the catalyst droplet on the tip of the NW and its corresponding EDX analysis. **a** EDX recorded on the catalyst particle, **b** EDX recorded on the interface between the catalyst and the NW,

c body of the NW, and **d** plot for the atomic percentage versus distance (nm) from the *top* of the catalyst droplet toward the body of the NW

NW growth, they can be used as the trackers to understand the nature of the catalyst during growth. In addition, the higher growth rate of (length of the NWs > 10 μm) GaN NWs grown for 30 min should exclude the speculation of pure VSS mechanism through solid catalytic droplet during growth. Together with the higher growth rate and Ni–Ga binary phase diagram, the growth is likely driven by VLS mechanism. However, this is quite different from

the classical VLS, in which for the growth of GaN NWs using Au as a catalyst, both the elements Ga and Au diffuse through the Au catalyst particle and the supersaturation in the catalyst leads to the crystallization at the liquid–solid interface (Yoo et al. 2006). Here, in the case of Ni-catalyst-assisted GaN NWs, Ga alone diffuses through the Ni catalyst and the N incorporation into the growing lattice takes place only through the triple phase interface because of unstable

N–Ni binary phase. However, we do not completely rule out the possibility of partial VSS mechanism (in addition with VLS mechanism) because the ex situ Ga composition measured by EDX is lower than 76 %, as required by the phase diagram to be in liquid state.

In order to probe the crystalline nature of the catalytic alloy and GaN NWs HRTEM analysis has been carried out. Figure 6a presents a detailed HRTEM examination on the interface between the NW and the catalyst droplet of a single GaN NW, which indicates that the interface is abrupt and smooth which supports the EDX data. HRTEM recorded on the catalyst droplet shows the presence of both crystalline and amorphous mixed phases of Ni–Ga. The lattice parameter (Fig. 6b) of the catalyst droplet (crystalline phase) is found to be ~ 3.5 Å, which is very similar to the lattice parameter of Ni_3Ga (Ducher et al. 2007). The crystalline nature of GaN NWs was further confirmed by SAED. Figure 6c shows SAED pattern, recorded perpendicular to the NW long axis. Detailed analysis of the diffraction pattern shows that the NW took the wurtzite structure and grew along [100] crystallographic direction. Figure 6d shows the NW is free of domain boundaries and cubic inclusion

having a single-crystalline nature. The NW diameter is apparently very homogeneous from top to bottom without any tapering effect. TEM and SAED observations over many NWs, and also at different locations of each NW showed similar diffraction pattern and lattice fringes oriented along [100] crystallographic direction.

The schematic illustration for the growth of GaN NWs with catalyst-assisted VLS is shown in Fig. 7. It is clearly represented that the Ga-radicals follow two path ways for the incorporation onto the growth site, first adatom diffusion through catalyst droplet and second adatom migration on the surface of the droplet and sidewalls of the wire through the interface. However, N-radicals, which have poor solubility in catalytic droplet, incorporate into the growing lattice only via the solid/liquid (NW/droplet) interface and not by means of diffusion through catalyst droplet.

Temperature-dependent photoluminescence for ensembles of GaN NWs measured at different temperature ranges is shown in Fig. 8a. Lorentz deconvoluted spectra show free donor-bound exciton (DBE) transition in wurtzite GaN at 3.467 eV for 10 K, with the FWHM (Full width at half maximum) of ~ 100 meV.

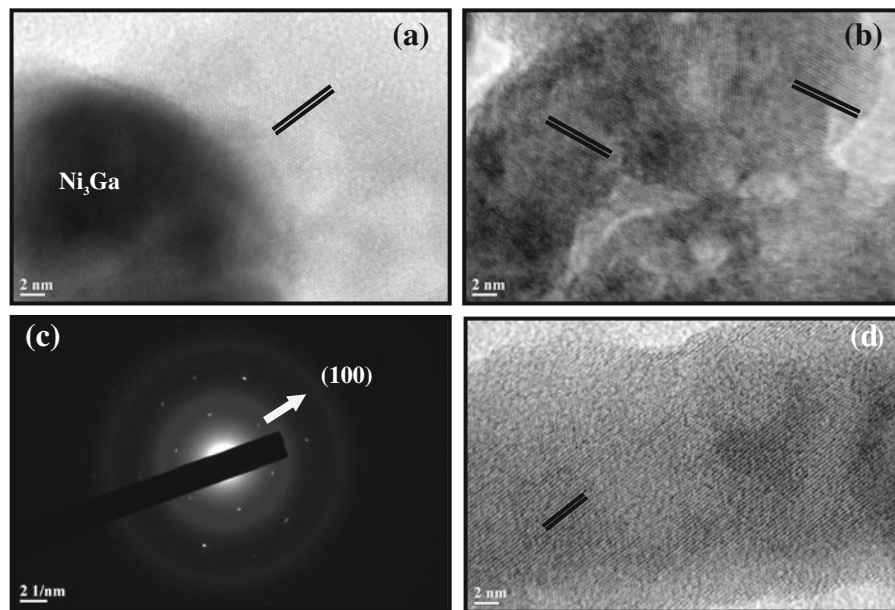


Fig. 6 **a** High-resolution TEM image of interface between the GaN NW and the Ni droplet. **b** High-resolution TEM images recorded on the droplet reveals that the droplet contains both the amorphous and crystalline phases. **c** Selected area electron

diffraction pattern on the body of the GaN NW shows the hexagonal crystalline nature of the NWs. **d** High-resolution TEM image recorded on the body of the NW shows the clearly visible lattice fringes

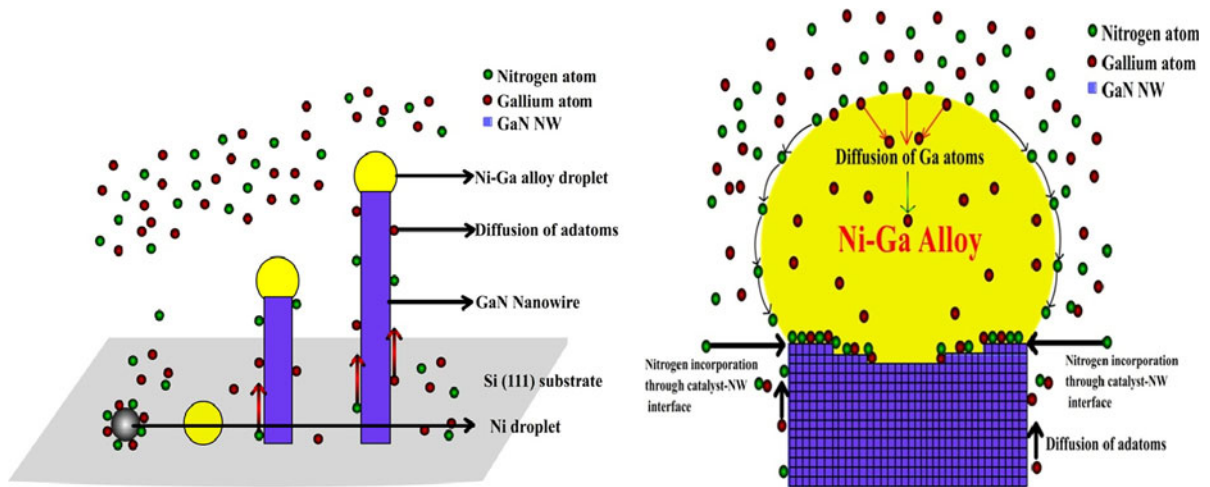


Fig. 7 **a** Schematic illustration for the growth of catalyst-assisted GaN NWs. **b** Shows the pathway for the incorporation of Ga and N into the growth lattice. It is obvious that Ga diffuses on catalyst, where N incorporation is through the triple phase boundary

As the temperature increases, its peak position shifts to lower energy and the peak approaches to 3.374 eV with the FWHM of 145 meV for 300 K. The crystalline quality of Ni-catalytic-assisted GaN NWs is quite good as compared with CVD grown GaN NWs (Yoo et al. 2006). The dominant emission at 3.326 eV for 10 K is attributed to donor–acceptor pair (DAP) band. The DAP band quenches at temperatures above ~ 150 K, and typically suppressed at room temperature. There are no other detectable emissions from the NWs, which confirm that the NWs are free from the defects such as V_{Ga} , V_{N} , and complex defects related that gives rise to emission of yellow luminescence (YL) at 2.2 eV, which is the characteristic emission of GaN grown by different methods, including MBE (Reshchikova and Morkoc 2005; Meijers et al. 2006). Using the Varshni formula (Uchida et al. 1999) and band-tail model, the temperature-dependent emission energy can be fitted by

$$E_{\text{g}}(T) = E_{\text{g}}(0) - \left(\frac{\alpha T^2}{T + \beta} \right) \quad (1)$$

where $E(0)$ is the emission energy at 0 K. α and β are fitting parameters to be determined by curve fitting to the experimental data. The results of the best fit are represented by red line. Figure 8b shows the Varshini fitting for the energy of DBE peak at various temperatures. The fitting parameters are $E_{\text{g}}(0) = 3.469$ eV, $\alpha = 5.63 \times 10^{-4}$ eV K $^{-1}$, and $\beta = 224.62$ K. The value of $E_{\text{g}}(0)$ for the free exciton emission is estimated

to be 3.469 eV and agrees well with the reported value of GaN bulk crystal (Hashimoto et al. 2004). Figure 8c shows an Arrhenius plot of the integrated PL intensity of DBE peak over a broad temperature range. The quenching of the PL luminescence with temperature is attributed to the thermal emission of the photo carriers that escaped the local potential minima caused by potential fluctuations, such surface roughness. Hence, the activation energy can be correlated with the degree of the exciton confinement. The following expression is generally used to calculate the activation energy (E_{a}) in thermally activated processes (Li et al. 2001).

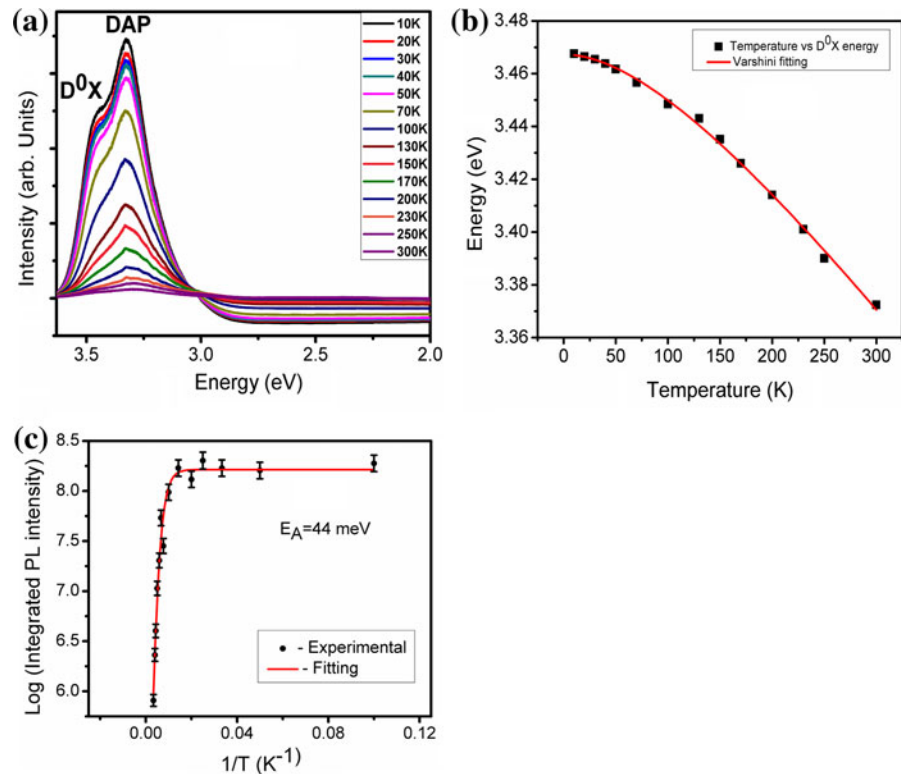
$$I(T) = \frac{I(0)}{(1 + A * \exp(-E_{\text{a}}/KT))} \quad (2)$$

where $I(T)$ is the PL intensity at temperature T K, $I(0)$ is the PL intensity at 0 K, A is the constant describing the capture of carriers, E_{a} is the activation energy of the thermal quenching process, K is the Boltzmann constant, and T is a thermodynamic temperature. The activation energy (E_{a}) of the GaN NWs is 44 meV, and it is in good agreement with the reported value for bulk GaN (Leroux et al. 1999).

Conclusion

In summary, the quasi-aligned whiskered GaN NWs have been fabricated using Ni-catalyst-assisted VLS approach by thermal CVD. The average diameter and

Fig. 8 **a** Temperature-dependent photoluminescence recorded for the ensembles of GaN NWs. **b** Varshni fitting (Temperature vs. Energy in eV) for the D^0X peak of GaN NWs. **c** Arrhenius plot of integrated PL intensity for GaN NWs



length of the NWs are 120 nm and ~ 5 μ m, respectively. The catalytic droplet on the apex of the NW contains both Ni and Ga with the ratio of 3:1 having stable crystalline and amorphous phases of Ni_3Ga , which clearly enlightens that the nitrogen radicals incorporate at the solid–liquid interface to growing crystal lattice rather than the diffusion through catalytic Ni–Ga alloy droplet. Further, the absence of N in the catalytic droplet supports that the Ni–N phase is not stable. Despite the enhancement of growth of one-dimensional GaN NWs by the presence of Ni–Ga alloy catalytic droplet at the apex of the NW, Ni does not migrate into GaN NWs. In addition, we have shown that III/V ratio is an important factor for the diameter-controlled vertical growth of GaN NWs. The growth rate is found to be independent of wire diameter and high supersaturation in the growth regime account for this unusual property. The temperature-dependent PL spectrum indicates that the GaN NWs have excellent optical quality with the absence of defect-induced yellow luminescence at 2.2 eV. The activation energy of GaN NWs is calculated to be ~ 44 meV from the Arrhenius plot.

Acknowledgments One of the authors K.J thanks Department of Science and Technology (DST), Govt. of India for the financial assistances under Project No. SR/FTP/PS-64/2007 and SR/NM/NS-77/2008. V.P acknowledges CSIR, Govt. of India for the award of senior research fellowship (SRF). Authors acknowledge Dr. P.V. Satyam, Institute of Physics, Bhubaneswar, India for TEM measurements. Author V. P acknowledges P. Sundara Venkatesh and R. Parameshwari for the technical assistance and fruitful discussions.

References

- Byeun Y, Han K, Choi SC (2006) Single crystal growth of one-dimensional GaN nanostructures by halide vapor-phase epitaxy. *J Electroceram* 17(24):903–907
- Cai XM, Djurišić AB, Xie MH (2006) GaN nanowires: CVD synthesis and properties. *Thin Solid Films* 515(3):984–989
- Cui Y, Zhong Z, Wang D, Wang WU, Lieber CM (2003) High performance silicon nanowire field effect transistors. *Nano Lett* 3(2):149–152
- Chèze C, Geelhaar L, Brandt O, Weber WM, Riechert H, Münch S, Rothmund R, Reitzenstein R, Forchel A, Kehagias T, Komninou P, Dimitrakopoulos GP, Karakostas T (2010a) Direct comparison of catalyst-free and catalyst-induced GaN nanowires. *Nano Res* 3:528–536
- Chèze C, Geelhaar L, Trampert A, Brandt O, Weber WM, Riechert H (2010b) Collector phase transitions during

- vapor–solid–solid nucleation of GaN nanowires. *Nano Lett* 10(9):3426–3431
- Chèze C, Geelhaar L, Jenichen B, Riechert H (2010c) Different growth rates for catalyst-induced and self-induced GaN nanowires. *Appl Phys Lett* 97:153105
- Debnath RK, Meijers R, Richter T, Stoica T, Calarco R, Lüth H (2007) Mechanism of molecular beam epitaxy growth of GaN nanowires on Si(111). *Appl Phys. Lett* 90:123117
- Diaz RE, Sharma R, Jarvis K, Zhanga Q, Mahajan S (2012) Direct observation of nucleation and early stages of growth of GaN nanowires. *J Cryst Growth* 341:1–6
- Duan X, Huang Y, Cui Y, Wang J, Lieber CM (2001) Indium phosphide nanowires as building blocks for nanoscale electronic and optoelectronic devices. *Nature* 409:66–69
- Duan X, Huang Y, Agarwal R, Lieber CM (2003) Single-nanowire electrically driven lasers. *Nature* 421:241–245
- Dubrovskii VG, Sibirev NV, Cirlin GE, Soshnikov IP, Chen WH, Larde R, Cadel E, Pareige P, Xu T, Gridier B, Nys JP, Stievenard D, Moewe M, Chuang LC, Chang-Hasnain C (2009) Gibbs–Thomson and diffusion-induced contributions to the growth rate of Si, InP, and GaAs nanowires. *Phys Rev. B* 79:205316
- Ducher R, Kainuma R, Ishida K (2007) Phase equilibria in the Ni-rich portion of the Ni–Ga binary system. *Intermetallics* 15:148–153
- Geelhaar L, Chèze C, Weber WM, Averbeck R, Riechert H, Kehagias Th, Komninou Ph, Dimitrakopoulos GP, Karakostas Th (2007) Axial and radial growth of Ni-induced GaN nanowires. *Appl Phys Lett* 91:093113
- Gradecak S, Qian F, Li Y, Park HG, Lieber CM (2005) GaN nanowire lasers with low lasing thresholds. *Appl Phys Lett* 87:173111
- Gröbner J, Wenzel R, Fischer GG, Schmid-Fetzer RJ (1999) Thermodynamic calculation of the binary systems M–Ga and investigation of ternary M–Ga–N phase equilibria ($M = \text{Ni, Co, Pd, Cr}$). *J Phase Equilibria* 20(6):615–625
- Harm JC, Tcherynycheva M, Patriarche G, Travers L, Glas F, Cirlin G (2007) GaAs nanowires formed by Au-assisted molecular beam epitaxy: effect of growth temperature. *J Cryst Growth* 301:853–856
- Hashimoto M, Tanaka H, Asano R, Hasegawa S, Asahi H (2004) Observation of photoluminescence emission in ferromagnetic semiconductor GaCrN. *Appl Phys Lett* 84(21):4191–4193
- Huang Y, Duan X, Cui Y, Lieber CM (2002) Nonvolatile memory and programmable logic from molecule-gated nanowires. *Nano Lett* 2(5):487–490
- Kodambaka S, Tersoff J, Reuter MC, Ross FM (2006) Diameter-independent kinetics in the vapor–liquid–solid growth of Si nanowires. *Phys Rev Lett* 96:096105
- Kuykendall T, Pauzauskie P, Lee S, Zhang Y, Goldberger J, Yang P (2003) Metalorganic chemical vapor deposition route to GaN nanowires with triangular cross sections. *Nano Lett* 3(8):1063–1066
- Lari L, Murray RT, Bullough TJ, Chalker PR, Gass M, Cheze C, Geelhaar L, Riechert H (2008) Nanoscale compositional analysis of Ni-based seed crystallites associated with GaN nanowire growth. *Physica E* 40:2457–2461
- Lekhal K, Avit G, Andre Y, Trassoudaine A, Gil E, Varenne C, Bougerol C, Monier G, Castellucci D (2012) Catalyst-assisted hydride vapor phase epitaxy of GaN nanowires: exceptional length and constant rod-like shape capability. *Nanotechnology* 23:405601
- Leroux M, Grjean N, Beaumont B, Nataf G, Semond F, Massies J, Gibart P (1999) Temperature quenching of photoluminescence intensities in undoped and doped GaN. *J Appl Phys* 86(7):3721–3728
- Li J, Nam KB, Kim KH, Lin JY, Jiang HX (2001) Growth and optical properties of $\text{In}_x\text{Al}_y\text{Ga}_{1-x-y}\text{N}$ quaternary alloys. *Appl Phys Lett* 78(1):61–63
- Meijers R, Richter T, Calarco R, Stoica T, Bochem HP, Marso M, Luth H (2006) GaN-nanowhiskers: MBE-growth conditions and optical properties. *J Cryst Growth* 289:381–386
- Ra YH, Navamathavan R, Park JH, Lee CR (2013) High-quality uniaxial $\text{In}_x\text{Ga}_{1-x}\text{N}/\text{GaN}$ multiple quantum well (MQW) nanowires (NWs) on Si(111) grown by metal-organic chemical vapor deposition (MOCVD) and light-emitting diode (LED) fabrication. *ACS Appl Mater Interfaces* 5:2111–2117
- Robins LH, Bertness KA, Barker JM, Sanford NA, Schlager JB (2007) Optical and structural study of GaN nanowires grown by catalyst-free molecular beam epitaxy. I: near-band-edge luminescence and strain effects. *J Appl Phys* 101:113505
- Roper SM, Anderson AM, Davis SH, Voorhees PW (2010) Radius selection and droplet unpinning in vapor–liquid–solid-grown nanowires. *J Appl Phys* 107:114320
- Reshchikova MA, Morkoc H (2005) Luminescence properties of defects in GaN. *J Appl Phys* 97:061301
- Seifert W, Borgstrom M, Deppert K, Dick KA, Johansson J, Larsson MW, Martensson T, Skold N, Svensson CPT, Wacaser BA, Wallenberg LR, Samuelson L (2004) Growth of one-dimensional nanostructures in MOVPE. *J Cryst Growth* 272:211–220
- Stoica T, Sutter E, Meijers RJ, Debnath RK, Calarco R, Luth H, Grutzmacher D (2008) Interface and wetting layer effect on the catalyst-free nucleation and growth of GaN nanowires. *Small* 4(6):751–754
- Uchida K, Tang T, Goto S, Mishima T, Niwa A, Gotoh JJ (1999) Spiral growth of InGaN/InGaN quantum wells due to Si doping in the barrier layers. *Appl Phys Lett* 74(8):1153–1155
- Venugopalan HS, Mohny SE, Luther BP, Wolter SD, Redwing JM (1997) Interfacial reactions between nickel thin films and GaN. *J Appl Phys* 82(2):650–654
- Wagner RS, Ellis WC (1964) Vapor–liquid–solid mechanism of single crystal growth. *Appl Phys Lett* 4(5):89–90
- Wen CY, Reuter MC, Bruley J, Tersoff J, Kodambaka S, Stach EA, Ross FM (2009) Formation of compositionally abrupt heterojunctions in silicon-germanium nanowires. *Science* 326(5957):1247–1250
- Weng X, Burke RA, Redwing JM (2009) The nature of catalyst particles and growth mechanisms of GaN nanowires grown by Ni-assisted metal–organic chemical vapor deposition. *Nanotechnology* 20:085610
- Wriedt HA, Nash P (1991) Phase diagrams of binary nickel alloys. ASM International, Materials Park, pp 213–216
- Yan R, Gargas D, Yang P (2009) Nanowire photonics. *Nat Photonics* 3:569–576
- Yoo J, Hong YJ, An SJ, Yi CB, Joo T, Kim JW, Lee JS (2006) Photoluminescent characteristics of Ni-catalyzed GaN nanowires. *Appl Phys Lett* 89:043124
- Zhou X, Chesin J, Crawford S, Gradecak S (2012) Using seed particle composition to control structural and optical properties of GaN nanowires. *Nanotechnology* 23:285603